Interplay of Rotational, Relaxational, and Shear Dynamics in Solid ^{4}He

E. J. Pratt, *et al.*

Science **332**, 821 (2011);
DOI: 10.1126/science.1203080

3. T. Kortemme *et al.*, *Nat. Struct. Mol. Biol.* **11**, 371 (2004).
4. R. K. Jha *et al.*, *J. Mol. Biol.* **400**, 257 (2010).
5. P. S. Huang, J. J. Love, S. L. Mayo, *Protein Sci.* **16**, 2770 (2007).
6. J. Karanicolas *et al.*, *Mol. Cell* **42**, 250 (2011).
7. S. Liu *et al.*, *Proc. Natl. Acad. Sci. U.S.A.* **104**, 5330 (2007).
8. Writing Committee of the WHO Consultation on Clinical Aspects of Pandemic (H1N1) 2009 Influenza, *N. Engl. J. Med.* **362**, 1708 (2010).
9. J. Sui *et al.*, *Nat. Struct. Mol. Biol.* **16**, 265 (2009).
10. D. C. Ekiert *et al.*, *Science* **324**, 246 (2009).
11. Group 1 includes 10 of the 16 HA subtypes: H1, H2, H5, H6, H8, H9, H11, H12, H13, and H16. Group 2 includes the remaining six subtypes: H3, H4, H7, H10, H14, and H15.
12. L. Lo Conte, C. Chothia, J. Janin, *J. Mol. Biol.* **285**, 2177 (1999).
13. T. Clackson, J. A. Wells, *Science* **267**, 383 (1995).
14. Materials and methods are available as supporting material on *Science* Online.
15. M. G. Rossmann, *J. Biol. Chem.* **264**, 14587 (1989).
16. J. Chen, J. J. Skehel, D. C. Wiley, *Proc. Natl. Acad. Sci. U.S.A.* **96**, 8967 (1999).
17. The other hot spot residues (HS1 and HS2) differed from the side chains observed in the crystal structures in their conformation or identity. Each hot spot residue was further diversified by constructing all conformations, the terminal atoms of which coincided with those modeled above. For instance, for HS3, these consisted of all Tyr conformations that matched the position of the aromatic ring and hydrogen bond. This diversification step produced a "fan" of backbone positions for each residue in the hot spot libraries.
18. Proteins in the scaffold set contained no disulfides, were expressed in *E. coli*, and were predicted to form monomers (*14*).
19. D. Schneidman-Duhovny, Y. Inbar, R. Nussinov, H. J. Wolfson, *Nucleic Acids Res.* **33** (Web Server issue), W363 (2005).
20. J. J. Gray *et al.*, *J. Mol. Biol.* **331**, 281 (2003).
21. B. Kuhlman *et al.*, *Science* **302**, 1364 (2003).
22. G. Chao *et al.*, *Nat. Protoc.* **1**, 755 (2006).
23. A third design HB35 bound HA at apparent low-micromolar affinity; however, binding was only partially abolished upon coincubation of HA with the CR6261 Fab, which indicated, at most, partial contact with the target surface on the stem region of HA, and so this design was eliminated from further consideration (fig. S7). A handful of other designs bound HA, albeit weakly and with incomplete reproducibility (*14*).
24. We recorded dissociation constants using two main methods: by titration of HA against yeast surface-displayed designs and by fitting both kinetic and equilibrium measurements using surface plasmon resonance. As there is a discrepancy in determining K_d values between the methods, measurements derived from yeast surface-display titrations are listed as apparent K_d and should be viewed qualitatively (*14*).
25. C. E. Stevenson *et al.*, *Proteins* **65**, 1041 (2006).
26. R. Das, D. Baker, *Annu. Rev. Biochem.* **77**, 363 (2008).
27. The alanine-scan mutations were as follows: for HB36.3, Phe^{49}, Met^{53}, and Trp^{57}; for HB80.1 Phe^{13}, Phe^{25}, and Tyr^{40} (table S4 and SOM text).
28. HB36.3 was not able to block the pH-induced conformational changes in the H1 and H5 HAs under identical assay conditions, even though HB36.3 and HB80.3 have very similar dissociation constants and kinetic off-rates at pH 7.5 (fig. S12 and SOM text).
29. Single-letter abbreviations for the amino acid residues are as follows: A, Ala; C, Cys; D, Asp; E, Glu; F, Phe; G, Gly; H, His; I, Ile; K, Lys; L, Leu; M, Met; N, Asn; P, Pro; Q, Gln; R, Arg; S, Ser; T, Thr; V, Val; W, Trp; and Y, Tyr.

Acknowledgments. Computational designs were generated on resources generously provided by participants of Rosetta @ Home and the Argonne National Leadership Computing Facility. We thank J. L. Gallaher for protein preparation. S.J.F. was supported by a long-term fellowship from the Human Frontier Science Program, J.E.C. was supported by the Jane Coffin Childs Memorial Fund, and E.M.S. by a career development award from the National Institute of Allergy and Infectious Diseases, NIH, AI057141. Research in the Baker laboratory was supported by grants from the Defense Advanced Research Projects Agency, the NIH yeast resource center, the Defense Threat Reduction Agency, and the Howard Hughes Medical Institute and in the Wilson laboratory by NIH AI058113, predoctoral fellowships from the Achievement Rewards for College Scientists Foundation and the NIH Molecular Evolution Training Program GM080209 (D.C.E.), and the Skaggs Institute for Chemical Biology. X-ray diffraction data sets were collected at the Stanford Synchrotron Radiation Lightsource beamline 9-2 and at the Advanced Photon Source (APS) beamline 23ID-B (GM/CA-CAT). The GM/CA CAT 23-ID-B beamline has been funded in whole or in part with federal funds from National Cancer Institute (Y1-CO-1020) and the National Institute of General Medical Science, NIH (Y1-GM-1104). Use of the APS was supported by the U.S. Department of Energy, Basic Energy Sciences, Office of Science, under contract no. DE-AC02-06CH11357. Coordinates and structure factors were deposited in the Protein Data Bank as entry 3R2X.

Supporting Online Material

www.sciencemag.org/cgi/content/full/332/6031/816/DC1
Materials and Methods
SOM Text
Figs. S1 to S12
Tables S1 to S7
References

7 January 2011; accepted 8 April 2011
10.1126/science.1202617

Interplay of Rotational, Relaxational, and Shear Dynamics in Solid ^{4}He

E. J. Pratt,[1,2]* B. Hunt,[1,3]* V. Gadagkar,[1] M. Yamashita,[4] M. J. Graf,[5] A. V. Balatsky,[5] J. C. Davis[1,6,7]†

Using a high-sensitivity torsional oscillator (TO) technique, we mapped the rotational and relaxational dynamics of solid helium-4 (^{4}He) throughout the parameter range of the proposed supersolidity. We found evidence that the same microscopic excitations controlling the torsional oscillator motions are generated independently by thermal and mechanical stimulation. Moreover, a measure for the relaxation times of these excitations diverges smoothly without any indication for a critical temperature or critical velocity of a supersolid transition. Finally, we demonstrated that the combined temperature-velocity dependence of the TO response is indistinguishable from the combined temperature-strain dependence of the solid's shear modulus. This implies that the rotational responses of solid ^{4}He attributed to supersolidity are associated with generation of the same microscopic excitations as those produced by direct shear strain.

Solid ^{4}He may become a supersolid (*1*) when its temperature T and mass-flow velocity V fall below their critical (*2*) values T_c and V_c. Indeed, torsional oscillator (TO) studies (*3*, *4*) reveal that the resonant angular frequency of rotation ω increases rapidly below both $T \sim 250$ mK and rim velocity $V \sim 10^{-4}$ ms^{-1}, as if superfluid inertia decouples at a critical temperature and velocity. These ω increases (*3*–*10*) are greatly diminished by blocking the TO annulus (*4*, *11*), as if superfluid inertia is thereby reconnected. Signatures in the heat capacity ascribed to supersolidity also occur in this same temperature range (*12*). However, direct mass-flow studies detect maximum currents that are far smaller than those implied by the TO experiments (*13*–*15*). Moreover, the temperature dependence of the resonance frequency $f(T) = \omega(T)/2\pi$ of TOs containing solid ^{4}He (*3*–*11*) resembles closely that of its shear modulus $\mu(T)$ (*16*). Coincident with the maximum rates of increase of $f(T)$ and $\mu(T)$ are maxima in TO dissipation (*4*–*6*, *8*, *9*) and shear dissipation (*16*, *17*), respectively. Such effects should not exist during a bulk Bose-Einstein condensation transition, although they do occur in the Berezinskii-Kosterlitz-Thouless (BKT) transition of a superfluid film (*18*) [see Supporting Online Material (SOM) section I (*19*)]. Finally, the increases in both f and μ are quickly extinguished by increasing TO maximum rim velocity V (*3*–*8*, *10*) or shear strain ε (*16*, *20*), respectively.

Several theoretical models have been proposed to explain the unexpectedly complex rotational dynamics of solid ^{4}He. The first is a simple supersolid (*1*) in which Bose-Einstein condensation of vacancies produces an inter-

[1]Laboratory for Atomic and Solid State Physics, Department of Physics, Cornell University, Ithaca, NY 14853, USA. [2]Kavli Institute for Theoretical Physics, University of California, Santa Barbara, CA 93016, USA. [3]Department of Physics, Massachusetts Institute of Technology, Cambridge, MA 02139, USA. [4]Department of Physics, Kyoto University, Kyoto 606-8502, Japan. [5]Theoretical Division and Center for Integrated Nanotechnologies, Los Alamos National Laboratory, Los Alamos, NM 87545, USA. [6]Condensed Matter Physics and Materials Science Department, Brookhaven National Laboratory, Upton, NY 11973, USA. [7]School of Physics and Astronomy, University of St. Andrews, St. Andrews, Fife KY16 9SS, UK.

*These authors contributed equally to this work.
†To whom correspondence should be addressed. E-mail: jcdavis@ccmr.cornell.edu

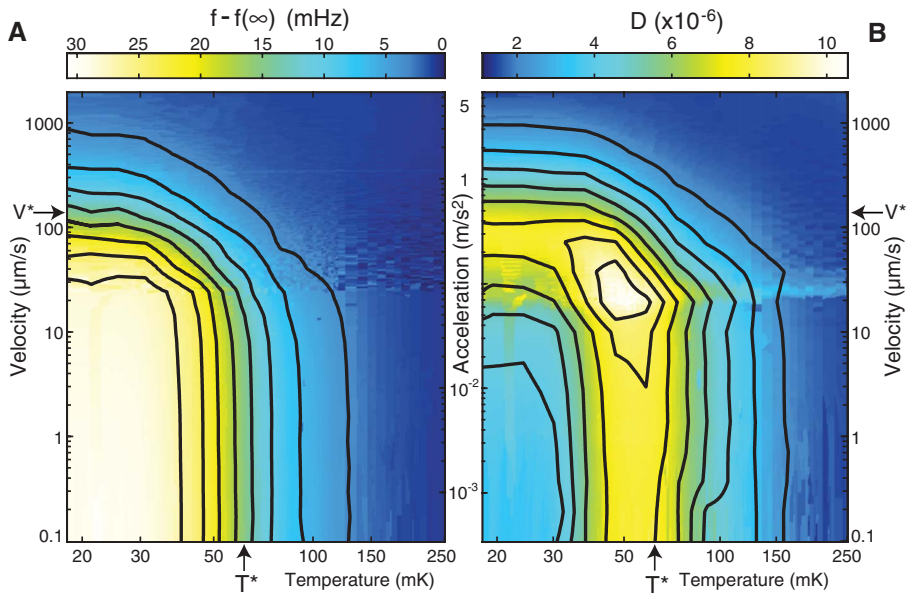

Fig. 1. TO resonant frequency shift $f(T)$ (**A**) and dissipation data (**B**) mapped throughout the V-T plane. Ninety-eight free inertial decay curves (each at a different temperature) were smoothly interpolated into the two color-coded surfaces displayed here on identical log-log axes. The low-velocity maximum frequency shift (~30 mHz) would correspond to a superfluid fraction of 5.6%.

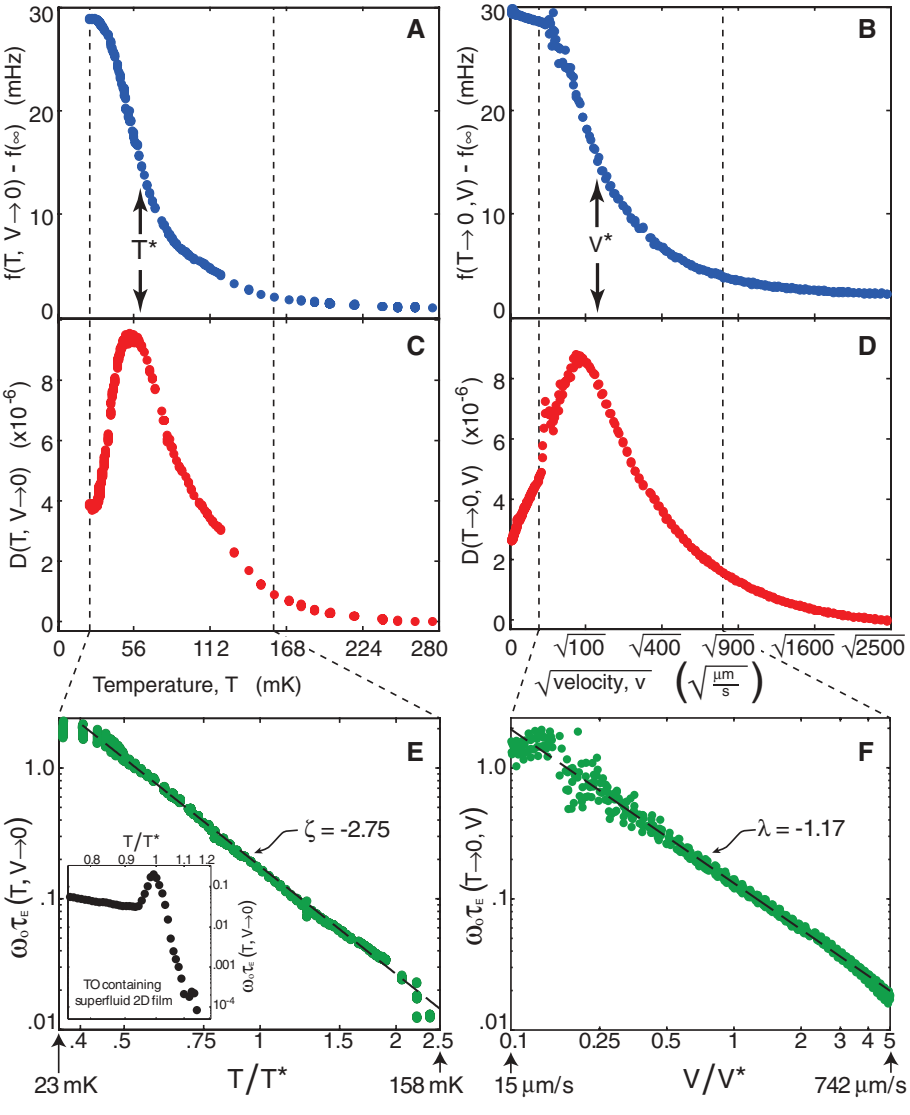

Fig. 2. (**A**) TO resonant frequency shift $f(T)$ measured at lowest rim velocity. T^* is defined as the temperature at which 50% of the frequency change has occurred (Fig. 1). (**B**) TO resonant frequency shift $f(\sqrt{V})$ measured at lowest temperature. V^* is defined as the rim velocity at which 50% of the frequency change has occurred (Fig. 1). (**C**) TO dissipation $D(T)$ measured at lowest rim velocity. (**D**) TO dissipation $D(\sqrt{V})$ measured at lowest temperature. (**E**) The empirical measure of microscopic relaxation times $\omega_0\tau_E(T)|_{V\to 0}$ from data in Fig. 2, A and C. The inset shows the equivalent analysis using Eq. 3 for the BKT transition of a superfluid ^{4}He film (see SOM section I). (**F**) The empirical measure of microscopic relaxation times $\omega_0\tau_E(V)|_{T\to 0}$ from data in Fig. 2, B and D. It diverges smoothly as V^{λ} with $\lambda = -1.17 \pm 0.05$.

penetrating superfluid with well-defined T_c and V_c. The second is an incipient supersolid lacking long-range phase coherence (*21*, *22*). A third class of model posits disorder-induced superfluidity (*9*, *23*–*29*). The final proposal is that solid ^{4}He contains a population of inertially active crystal excitations (*30*–*35*), whose relaxation time τ lengthens smoothly with falling T and V. These excitations are variously proposed to be a dynamical network of pinned dislocations (*17*, *30*, *35*), atomic-scale tunneling two-level systems (*34*), or the glassy response of defects distributed throughout the solid (*31*–*33*). All models positing inertially active crystal excitations have the property that, as $\tau(T)$ passes through the condition $\omega\tau = 1$, a strong maximum in $|df/dT|$ and TO dissipation D should occur (*9*, *31*–*35*), even though there is no supersolid T_c and V_c. By contrast, a bulk superfluid phase transition should exhibit clear signatures of both T_c and V_c (*2*). One way to distinguish between such models is to determine the evolution of microscopic relaxational time constants τ, in search of either the smoothly diverging τ of a system governed by $\omega\tau = 1$ phenomenology or the sudden changes expected in τ at a thermodynamic T_c and/or V_c.

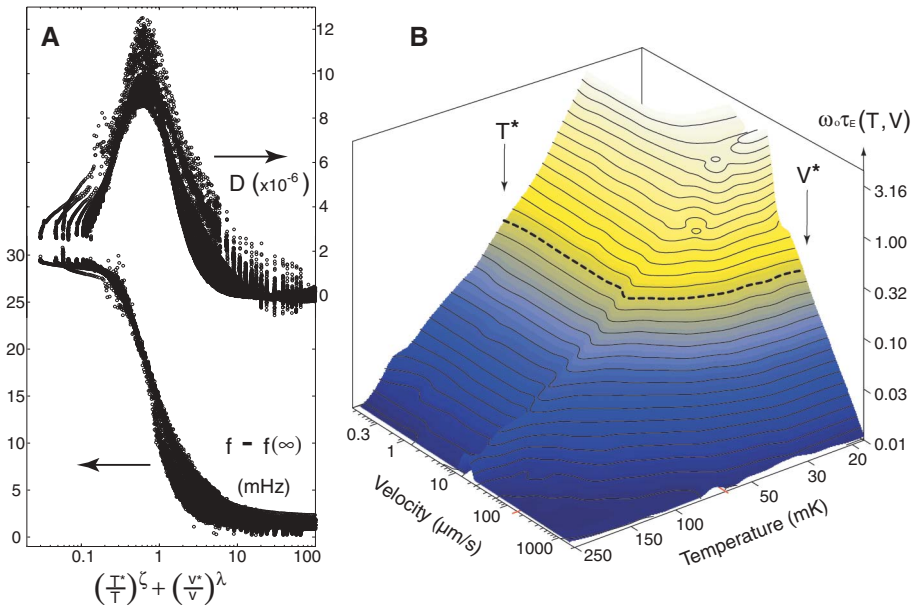

Fig. 3. (**A**) All of the TO dynamical responses throughout the *V*-*T* plane [$f(T,V)$ from Fig. 1A and $D(T,V)$ from Fig. 1B] are collapsed onto just two curves (very similar in structure to the $\mathrm{Re}(\chi^{-1})$ and $\mathrm{Im}(\chi^{-1})$ components of the Debye susceptibility) by plotting $f[(T^*/T)^\zeta + (V^*/V)^\lambda]$ and $D[(T^*/T)^\zeta + (V^*/V)^\lambda]$ (SOM section IV). Here, we find that $\mathrm{Re}(\chi^{-1}) \propto f[(T^*/T)^\zeta + (V^*/V)^\lambda]$ is always too large, in comparison with $\mathrm{Im}(\chi^{-1}) \propto D[(T^*/T)^\zeta + (V^*/V)^\lambda]$, to be explained quantitatively by a Debye susceptibility model; this point has been used to motivate a "superglass" hypothesis (*9*). (**B**) A comprehensive map of empirical relaxation times $\omega_0\tau_E(T,V)$ deduced using Eq. 3 represented as a surface in the log*T*-log*V* plane. The equally spaced contour lines in log $\omega_0 t_E(T,V)$ reveal the underlying divergence of $\omega_0\tau_E(T,V)$ as combined power laws $[(T^*/T)^\zeta + (V^*/V)^\lambda]$.

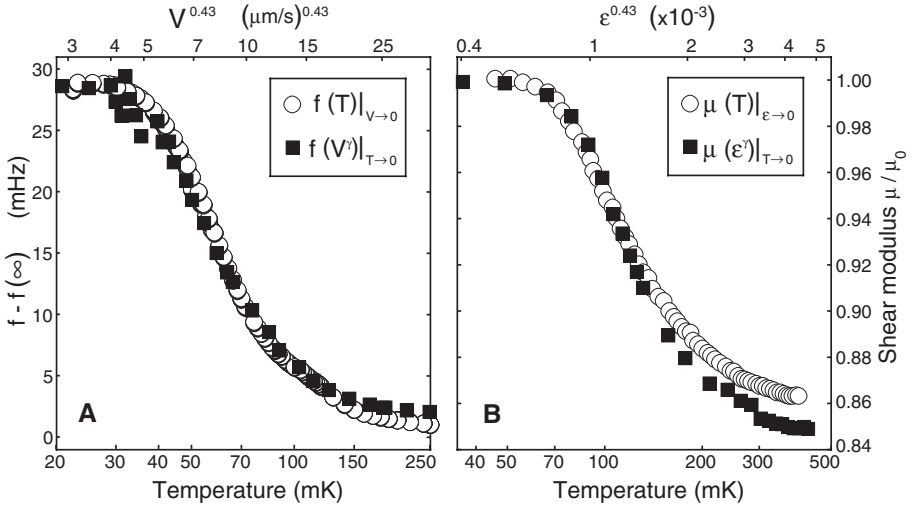

Fig. 4. (**A**) Plots of our simultaneously measured $f(T)|_{V\to0}$ (open circles) and $f(V^\gamma)|_{T\to0}$ (filled squares) from Figs. 1 and 2. (**B**) Simultaneous plots of measured $\mu(T)|_{\varepsilon\to0}$ (open circles) and $\mu(\varepsilon^\gamma)|_{T\to0}$ (filled squares) from (*20*) acquired at 2000 Hz.

An unbiased approach to TO studies of solid ^{4}He can be achieved by using the TO rotational susceptibility $\chi(\omega,T) = \theta(\omega,T)/\Gamma(\omega)$ (*9*). Here, $\theta(\omega,T)$ represents the amplitude of angular displacement as a function of ω and T in response to a harmonic torque $\Gamma(\omega)$ of constant magnitude. Then (*31*–*33*)

$$\chi^{-1}(\omega,T) = K - I\omega^2 - i\gamma\omega - \chi_{4He}^{-1}(\omega,T) \quad (1)$$

represents the properties of the bare TO plus the "back action" of the solid ^{4}He upon it through the solid's rotational susceptibility $\chi_{4He}^{-1}(\omega,T)$. Here, I is the combined moment of inertia of the TO plus ^{4}He at zero temperature, K is the torsional spring constant, and γ is the TO damping constant. To clarify these concepts, we consider a Debye rotational susceptibility $\chi_{4He}^{-1}(T) = g/[1 - i\omega_0\tau(T)]$ (*9*, *31*–*33*) with relaxational time constants $\tau(T)$ increasing with decreasing T. For this susceptibility

$$\frac{\mathrm{Im}(\chi_{4He}^{-1})}{\mathrm{Re}(\chi_{4He}^{-1})} = \frac{D(T)f(0)}{2[f(0) - f(T)]} = \omega_0\tau(T) \quad (2)$$

where $\mathrm{Re}(\chi_{4He}^{-1})$ and $\mathrm{Im}(\chi_{4He}^{-1})$ are its real and imaginary parts, respectively (*32*), and $D(T) = Q^{-1}(T) - Q^{-1}(T\to\infty)$ is the inverse contribution to the TO quality factor Q from the solid ^{4}He. Access to $\tau(T)$ for the microscopic excitations is therefore possible in principle from measurements of $\mathrm{Re}(\chi_{4He}^{-1})$ and $\mathrm{Im}(\chi_{4He}^{-1})$.

Following this approach, we mapped the rotational susceptibility of a TO containing solid ^{4}He throughout the *V*-*T* plane (SOM section II). The results in Fig. 1, A and B, reveal immediately that the frequency increase and dissipation peak are bounded by closely corresponding *V*-*T* contours. Thus, the same unexplained dissipation seen with falling temperature near the proposed supersolid T_c is found also with diminishing V in the range of the proposed (*3*, *4*) supersolid V_c. The highly similar contours of both $f(T,V)$ and $D(T,V)$ also reveal that the maxima in $|df/dT|$ and D are always linked, as if controlled by some combined function of T and V. Similar results were observed in all three distinct solid ^{4}He samples studied.

Next, we compared the solid ^{4}He rotational dynamics versus T as $V\to0$ to those versus $V^{0.5}$ as $T\to0$ (the rationale for $V^{0.5}$ will become clear below). Figure 2, A and C, shows $f(T)|_{V\to0}$ and $D(T)|_{V\to0}$, whereas Fig. 2, B and D, shows $f(V)|_{T\to0}$ and $D(V)|_{T\to0}$ (Fig. 1 data used are identified in fig. S5). Figure 2 reveals a striking and unexpected similarity between the results of what, for a simple superfluid, would be two com-

pletely different experiments (one stimulating the sample thermally and the other mechanically). To examine this, we define an empirical measure τ_E of relaxation times for any combination of T and V.

$$\tau_E(T,V) = \frac{D(T,V)\, f(0)}{2\omega_0[\, f(0) - f(T,V)]} \qquad (3)$$

In Fig. 2E, we show $\log\tau_E(T)$ plotted versus $\log(T/T^*)$ for the lowest rim velocity data (Fig. 2, A and C). In Fig. 2F, $\log\tau_E(V)$ is likewise plotted versus $\log(V/V^*)$ for the lowest temperature data (Figs. 2, B and D). Here, we define T^* and V^* as the temperature and rim velocity, respectively, at which half the total frequency shift has occurred (Fig. 1 and Fig. 2, A and B). This analysis reveals that the τ_E diverges smoothly as T^ζ with $\zeta = -2.75 \pm 0.1$ when $V \to 0$ and as V^λ with $\lambda = -1.17 \pm 0.05$ when $T \to 0$. Thus, the effects of temperature on $f(T)|_{V\to 0}$ and $D(T)|_{V\to 0}$ appear identical to those of rim velocity on $f(V^\gamma)|_{T\to 0}$ and $D(V^\gamma)|_{T\to 0}$, respectively, where $\gamma = \lambda/\zeta = 0.43$ is the ratio of power-law exponents. Figure 2, E and F, also shows that no matter how complex the actual rotational dynamics (Fig. 2, A to D), the peak in D is always canceled by the peak in $|df/dT|$ to produce smoothly diverging functions $\tau_E(T)|_{V\to 0}$ and $\tau_E(V)|_{T\to 0}$ (fig. S7). Microscopic relaxational processes represented by τ_E should change dramatically at a superfluid phase transition; an excellent example of this is seen in $\tau_E(T)$ at the BKT superfluid phase transition of liquid ^{4}He, shown in the inset to Fig. 2E (fig. S1). However, no indications of the sudden change that would signify the supersolid T_c or V_c exist in Fig. 2, E and F. Instead, τ_E exhibits everywhere the smooth divergence expected in $\omega\tau = 1$ models.

Figures 1 and 2 provide direct empirical evidence that the effects of T and V on the TO are intimately related to each other. One may therefore ask whether a single Debye-like rotational susceptibility could describe the whole V-T plane dynamics in Fig. 1 when the effects of V on the relaxation time τ are correctly incorporated. Hypothesizing a total relaxation rate $1/\tau(T,V)$ due to a combination of two effects

$$\frac{1}{\tau(T,V)} = \frac{1}{\tau(T)} + \frac{1}{\tau(V)} \qquad (4)$$

along with the knowledge that the overall phenomenology appears identical as a function of $T^\zeta|_{V\to 0}$ and $V^\lambda|_{T\to 0}$ (Fig. 2) and interpolates smoothly between these limits (Fig. 1), yields an ansatz.

$$\frac{1}{\tau(T,V)} = \frac{\Sigma}{T^\zeta} + \frac{\Lambda}{V^\lambda} \qquad (5)$$

Here, Σ and Λ quantify the relative contributions to the relaxation rate from thermally and mechanically stimulated excitations (SOM section IV). Figure 3A shows that by using this ansatz, virtually all the complex solid ^{4}He rotational dynamics in $f(T,V)$ and $D(T,V)$ of Fig. 1 can be collapsed onto just two functions, $\mathrm{Re}(\chi^{-1})$ and $\mathrm{Im}(\chi^{-1})$, merely by plotting $f[(T^*/T)^\zeta + (V^*/V)^\lambda]$ and $D[(T^*/T)^\zeta + (V^*/V)^\lambda]$. Moreover, this apparent unification of rotational dynamics implies that Eq. 3 could yield a comprehensive image of $\tau_E(T,V)$ throughout the V-T plane by dividing all the data in Fig. 1B by that in Fig. 1A, as shown in Fig. 3B. Although the proposed V-T ranges for a supersolid phase transition (*3*, *4*, *12*) are at or below the dashed T^*-V^* contour, the τ_E surface exhibits everywhere the smoothly diverging relaxation processes expected in $\omega\tau = 1$ models. We emphasize here that all the above results (Figs. 1 to 3) are independent of any choice of $\chi^{-1}_{4He}(T,V)$ and therefore strongly constrain eventual microscopic models for the dynamics of solid ^{4}He.

Figures 1 and 2 provide evidence that the identical microscopic excitations are being generated by thermal and mechanical stimulation and that the overall rotational dynamics in $f(V,T)$ and $D(V,T)$ are consistent with a single $\omega\tau = 1$ mechanism that is controlled by a relaxation rate $(T^*/T)^\zeta + (V^*/V)^\lambda$ due to the combined influences from these two sources (Fig. 3). Because these unified dynamics also appear inconsistent with expectations for T_c or V_c of a superfluid transition (*2*), one must ask which model could account for them. Because the solid ^{4}He shear modulus $\mu(T)$ exhibits a very similar temperature dependence to $f(T)$ (*16*), and because this shear stiffening effect is extinguished by a characteristic strain as opposed to a critical velocity (*20*), a key question has been whether excitations generated by direct shearing are the same as those controlling the TO dynamics.

Our approach provides an opportunity to address this issue. If crystal excitations induced by inertial strain ε in the TO (where $\varepsilon \propto V$) are the cause of the anomalous rotational dynamics, then the indistinguishable structure of $f(T)|_{V\to 0}$ and $f(V^\gamma)|_{T\to 0}$ (Fig. 4A) should be mirrored by an equivalently indistinguishable relationship in shear modulus between $\mu(T)|_{\varepsilon\to 0}$ and $\mu(\varepsilon^\gamma)|_{T\to 0}$. When the measured μ from (*20*) is plotted simultaneously versus T and ε^γ in Fig. 4B (using the power-law ratio γ derived from our TO studies), this is precisely what we find. That the combined temperature-velocity dependence of the TO response mirrors quantitatively the combined temperature-strain dependence of the shear modulus, along with the original observation that $\mu(T)$ tracks $f(T)$ (*16*), implies that the rotational dynamics of solid ^{4}He are associated with the generation (presumably by inertial shearing) of the same type of microscopic excitations that are generated by direct shear strain ε. These conclusions appear to be in good accord with the observed smoothly diverging microscopic relaxation times as expected of $\omega\tau = 1$ models (Fig. 3) and with the absence of a signature in $\tau_E(T,V)$ for the T_c or V_c of a supersolid phase transition (Figs. 2 and 3). These results will motivate efforts to (i) identify directly whether the microscopic excitations are crystal dislocations as implied and (ii) determine whether they admit any associated zero-frequency contribution to the rotational susceptibility that would represent a superfluid component (*9*).

References and Notes

1. S. Balibar, *Nature* **464**, 176 (2010).
2. D. R. Tilley, J. Tilley, *Superfluidity and Superconductivity* (IOP, Bristol, UK, ed. 3, 1990).
3. E. Kim, M. H. W. Chan, *Nature* **427**, 225 (2004).
4. E. Kim, M. H. W. Chan, *Science* **305**, 1941 (2004).
5. A. S. C. Rittner, J. D. Reppy, *Phys. Rev. Lett.* **97**, 165301 (2006).
6. Y. Aoki, J. C. Graves, H. Kojima, *Phys. Rev. Lett.* **99**, 015301 (2007).
7. A. Penzev, Y. Yasuta, M. Kubota, *J. Low Temp. Phys.* **148**, 677 (2007).
8. M. Kondo, S. Takada, Y. Shibayama, K. Shirahama, *J. Low Temp. Phys.* **148**, 695 (2007).
9. B. Hunt *et al.*, *Science* **324**, 632 (2009).
10. H. Choi, S. Kwon, D. Y. Kim, E. Kim, *Nat. Phys.* **6**, 424 (2010).
11. A. S. C. Rittner, J. D. Reppy, *Phys. Rev. Lett.* **101**, 155301 (2008).
12. X. Lin, A. C. Clark, M. H. W. Chan, *Nature* **449**, 1025 (2007).
13. J. Day, J. Beamish, *Phys. Rev. Lett.* **96**, 105304 (2006).
14. S. Sasaki, R. Ishiguro, F. Caupin, H. J. Maris, S. Balibar, *Science* **313**, 1098 (2006).
15. M. W. Ray, R. B. Hallock, *Phys. Rev. Lett.* **100**, 235301 (2008).
16. J. Day, J. Beamish, *Nature* **450**, 853 (2007).
17. O. Syshchenko, J. Day, J. Beamish, *Phys. Rev. Lett.* **104**, 195301 (2010).
18. D. J. Bishop, J. D. Reppy, *Phys. Rev. Lett.* **40**, 1727 (1978).
19. Materials and methods are available as supporting material on *Science* Online.
20. J. Day, O. Syshchenko, J. Beamish, *Phys. Rev. Lett.* **104**, 075302 (2010).
21. P. W. Anderson, *Nat. Phys.* **3**, 160 (2007).
22. A. Penzev, Y. Yasuta, M. Kubota, *Phys. Rev. Lett.* **101**, 065301 (2008).
23. S. I. Shevchenko, *Sov. J. Low Temp. Phys.* **13**, 61 (1987).
24. M. Boninsegni *et al.*, *Phys. Rev. Lett.* **99**, 035301 (2007).
25. J. Wu, P. Phillips, *Phys. Rev. B* **78**, 014515 (2008).
26. J. Bossy, J. V. Pearce, H. Schober, H. R. Glyde, *Phys. Rev. B* **78**, 224507 (2008).
27. G. Biroli, C. Chamon, F. Zamponi, *Phys. Rev. B* **78**, 224306 (2008).
28. B. Svistunov, *Physica B* **404**, 521 (2009).
29. K.-M. Tam, S. Geraedts, S. Inglis, M. J. P. Gingras, R. G. Melko, *Phys. Rev. Lett.* **104**, 215301 (2010).
30. X. Rojas, A. Haziot, V. Bapst, S. Balibar, H. J. Maris, *Phys. Rev. Lett.* **105**, 145302 (2010).
31. A. V. Balatsky, M. J. Graf, Z. Nussinov, S. A. Trugman, *Phys. Rev. B* **75**, 094201 (2007).
32. Z. Nussinov, A. V. Balatsky, M. J. Graf, S. A. Trugman, *Phys. Rev. B* **76**, 014530 (2007).
33. M. J. Graf, Z. Nussinov, A. V. Balatsky, *J. Low Temp. Phys.* **158**, 550 (2010).
34. A. F. Andreev, *JETP Lett.* **85**, 585 (2007).
35. I. Iwasa, *Phys. Rev. B* **81**, 104527 (2010).

Acknowledgments: We are grateful for discussions and communications with J. Beamish, D. M. Ceperley, M. H. W. Chan, J. Day, A. T. Dorsey, R. B. Hallock, H. Kojima, D. M. Lee, A. J. Leggett, E. Mueller, D. R. Nelson, J. M. Parpia, N. V. Prokof'ev, J. D. Reppy, P. C. E. Stamp, B. Svistunov, and M. Troyer. These studies were supported by the National Science Foundation under grants DMR-0806629 and NSF PHY05-51164 to the Kavli Institute for Theoretical Physics. Work at Los Alamos was supported by U.S. Department of Energy grant DE-AC52-06NA25396 to the Center for Integrated Nanotechnologies and through the Laboratory Directed Research and Development program.

Supporting Online Material

www.sciencemag.org/cgi/content/full/332/6031/821/DC1
Materials and Methods
SOM Text
Figs. S1 to S7
References

19 January 2011; accepted 4 April 2011
10.1126/science.1203080